International Journal of Applied Earth Observation and Geoinformation 122 (2023) 103398

Contents lists available at ScienceDirect

International Journal of Applied Earth Observation and Geoinformation

journal homepage: www.elsevier.com/locate/jag

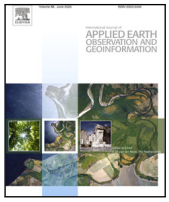

A multi-year land use trajectory strategy for non-active agricultural land mapping in sub-humid West Africa

Enzo Castro Alvarado [a,*], Agnès Bégué [a,b], Louise Leroux [c,d,e], Raffaele Gaetano [a,b]

[a] TETIS, Univ Montpellier, AgroParisTech, CIRAD, CNRS, INRAE, Montpellier, France
[b] CIRAD, UMR TETIS, F-34398 Montpellier, France
[c] CIRAD, UPR AIDA, F-34398 Montpellier, France
[d] AIDA, Univ Montpellier, CIRAD, Montpellier, France
[e] International Institute of Tropical Agriculture, Nairobi, Kenya

ARTICLE INFO

Keywords:
Fallow
Trajectory analysis
Sentinel-2
Supervised classification
Land use
Burkina Faso

ABSTRACT

Non-active agricultural land (NAAL) mapping in West Africa is essential to accurately assess agricultural systems and its contribution to food security and agro-ecological sustainability of current practices, and yet the available mapping methodologies are not adapted to the environmental and cropping conditions encountered when addressing tropical smallholder agriculture. In this study we present a strategy that makes use of Sentinel-2 image time series, CHIRPS monthly rainfall data and multiple years of in-situ data obtained from the JECAM database to map NAAL in a Soudanian site in Burkina Faso (Koumbia) between the years 2016 and 2021. In a first step we generated annual land use maps in four broad classes (managed, unmanaged, evergreen and non-vegetated) to detect fields being actively cultivated in a given year, and in a second step, we used these annual land use maps to differentiate non-active agricultural land by identifying shifts from one year to another. For the validation part, we analyzed the sensitivity of classification accuracy to in-situ data pre-processing by building 5 experimental validation data sets. The unmanaged classes F1-scores of the land use maps ranged between 0.86 and 0.98, depending on the year, whereas NAAL classes F1-scores ranged from 0.75 to 0.92 when validated against the most restrictive data set (pixels with no missing reference data for the period considered). NAAL represents between 7% to 14% of the study site cropland depending on the year. The higher class probabilities are in areas where data was available, whereas the low probabilities are localized and linked to transition areas on the outskirts of the department. Our results indicate that a multi-annual approach can allow NAAL mapping under challenging environments, yet efforts are to be made to develop more cost-efficient unsupervised solutions.

1. Introduction

Sub-Saharan agriculture is composed by a large proportion of smallholders where small cropping fields are common, often less than 1 hectare, defining a highly fragmented agricultural land, characterized by a high heterogeneity at the field level and where soil degradation, as well as a reduced and financially unaffordable access to mineral inputs and mechanization, limit crop production (Ruthenberg, 1974; Snapp et al., 2018; Tittonell and Giller, 2013). West African cropping systems have traditionally relied on long uncultivated periods of time to restore natural soil fertility, in some instances surpassing a decade between two periods of cultivation after which, the next cropping cycle is triggered by a removal and burning of all natural vegetation that has regrown during this idle period (slash-and-burn) (Ruthenberg, 1974; Manlay et al., 2000; Samaké et al., 2005; Faye et al., 2021; Zoungrana, 1993). However, the necessity to enhance the agricultural production, driven by a growing population (Vollset et al., 2020), has promoted a shift in cropping systems, which has been characterized by a reduction of fallow land and hence an increase of soil degradation. Quantification of the available active and non-active agricultural land (NAAL) is therefore not only key for a better estimation of the potential production in the region, but also for monitoring the sustainability, from an agro-ecological point of view, of the current intensification trends in local cropping practices.

Non-active agricultural land is often used as synonym of "fallow", which according to FAO's definition accounts to "the cultivated land that is not seeded for one or more growing seasons. The maximum idle period is usually less than five years" (FAO, 2022). Following this definition, what describes a fallow land is (a) the land has been

* Corresponding author.
E-mail address: enzo.castroalvarado@agroparistech.fr (E. Castro Alvarado).

https://doi.org/10.1016/j.jag.2023.103398
Received 3 March 2023; Received in revised form 15 June 2023; Accepted 20 June 2023
Available online 18 July 2023

previously cultivated, (b) the land is not currently being cultivated and (c) it is a temporary state that ends with a recultivation of land. This implies that the fallow land is actually defined by its past, current and future use rather than its sole current observable "land cover". However, more strict definitions also assume that (d) fallow fields exist as an agricultural practice within a cropping system as described in Bégué et al. (2018), which in turn implies that other abandoned agricultural land, due to reasons unrelated to cropping practices such as soil exhaustion, sociopolitical instability or simply manpower shortage should not be included within a strict sense "fallow" class. We could therefore establish that the idle period between two moments of observable active cropping is a necessary condition for validating a NAAL as "fallow" based exclusively on land cover data.

Satellite imagery has been proved to be a useful tool for generating land cover over broad regions such as *GlobCORINE* (Bontemps et al., 2009), *CGLS-LC100* (Buchhorn et al., 2020), or *Dynamic World* (Brown et al., 2022), allowing for a relatively economic solution and covering much larger areas compared to *in situ* surveys, and with continuous improvements in its spatio-temporal resolution. Nevertheless, NAAL mapping (or fallow land for that matter) has been, for the most part, disregarded by considering it an implicit part of a generic "cropland" class. Indeed, few studies propose specific methodologies for mapping and quantifying non-active agricultural land through the analysis of satellite imagery. These works are quite varied in terms of the spatial scale, from regional level in California (Wallace et al., 2017) or in China (Zhang et al., 2014), to entire countries (Qiu et al., 2022), continental scale (Estel et al., 2015, 2016) or target specific agro-climatic zones such as the Sahel in Africa (Tong et al., 2020). Almost all these attempts for differentiating non-active agricultural land are based on the hypothesis that fallow land exhibits a significantly different spectral signature during the growing season with respect to active cropland, and then implement a classification strategy based on machine learning algorithms (Tong et al., 2020, 2022; Estel et al., 2015; Rufin et al., 2022) or a rule-based system at an annual scale (Wallace et al., 2017; Qiu et al., 2022; Zhang et al., 2014). To the best of our knowledge, only few studies have implemented strategies using input data which exceed a single growing season for determining whether a field is being actively cropped or not. In these cases (Yin et al., 2018; Dara et al., 2018), decades of Landsat data are used for determining a cropland probability, and land use classes are subsequently determined by inflection points of this probability through time. Moreover, in more recent studies (Rufin et al., 2022; Tong et al., 2022) a complementary verification is performed for "fallow" fields, requiring them to being cultivated once on previous years. A particularly interesting approach is proposed in Zhao et al. (2023) to estimate the proportion of *abandoned cropland* (hence not targeting *fallow* land) in Yunnan province in China using long time-series of Landsat imagery and a trajectory analysis based on long term land use annual mapping. Thus, establishing a multi-year temporal relationship as a strategy for NAAL identification, either for generating reliable reference data sets or as part of their mapping methodology, appears to be a point of convergence for scientific community. Regardless of the strategy implemented, these approaches often rely on the use of a cropland mask to focus the analysis on arable land only : *GlobCORINE* map cropland class in Estel et al. (2015, 2016), *USDA-CDL* in Wallace et al. (2017) and Wu et al. (2014), or *CGLS-LC100* in Tong et al. (2020). Moreover, data acquisition for training and/or validation is based for the most part on photo-interpretation of high resolution imagery or relying on the availability of a single season *in situ* data collection.

Summarizing, most of the remote sensing-based methods require either (a) prior knowledge of cropland, (b) a crop/fallow reference data set obtained from ground surveys or through photo-interpretation, and (c) contrasted seasonal spectral signatures among the land cover and land use (LCLU) classes. The first requirement usually implies the use of accessible global cropland products. In West Africa, the accuracy of such products is generally low to moderate, depending on the farming system in place (Leroux et al., 2014) with below 70% user accuracy on best cases (Samasse et al., 2018; Xu et al., 2019). The second requirement must cope with the lack of reliable ground truth data, which is often insufficient in both time and space, or available imagery does not allow the visual recognition of small and heterogeneous crop/fallow fields. The third requirement is rarely verified in tropical West Africa, since most of crops are *rainfed*, hence exhibiting a phenological development during a period where optical remote sensing imagery is unlikely to be fully exploitable due to cloud coverage.

Thus, in this study we propose a NAAL mapping strategy that implements a series of methodological adaptation that can both (a) cope with technical limitations linked to tropical agriculture in West Africa, and (b) adapt to the multi-year nature of idle cropland, subject to either proper fallow practices or occasional short-term abandonment.

1.1. Proposed NAAL mapping strategy

Out of the described context, the purpose of this work is to investigate the issues for the design of a suitable methodology for mapping NAAL surfaces in areas where climate conditions, landscape fragmentation and heterogeneous cropping practices do not allow a thorough identification of agricultural land use/land cover. We start from the assumption that recent satellite missions such as ESA's Sentinel-2, delivering high-resolution and high frequency acquisitions in the optical multi-spectral domain over the globe, may indeed provide enough information to tackle some of these issues : (i) decametric spatial resolution can suitably address the spatial scale of the average field size in most of West African agrosystems, thus coping with landscape fragmentation issues, (ii) 5-day revisit time generally guarantees the acquisition of a sufficient number of images over a cropping season for tracking vegetation growth stages at field scale to some limited extent. Nonetheless, the diversity of cropping practices (sowing dates, cropping patterns, etc.) in conjunction with the local variability of the cropping conditions (soil, rainfall) may prevent the identification of specific agricultural land uses based on the sole image-derived spectral and temporal signatures (Inglada et al., 2015).

However, we are willing to tackle the identification of a specific agricultural land use (NAAL) which has an intrinsic multi-annual nature, since as stated before such use is determined by the fact that a given surface has been actively cultivated in past years. Matter of fact, rather than attempting to differentiate NAAL from other types of uses based on annual land cover data, a way to trigger the identification of NAAL is to detect, over multiple cropping seasons and over areas exhibiting seasonal vegetation life cycle (cropland-like), transitions between periods in which vegetation growth is *managed*, i.e. a cropping activity is actually performed, and periods in which it exhibits an *unmanaged* condition, which may happen for both NAAL and areas with natural deciduous/herbaceous vegetation. Based on the hypothesis that an annual time series of optical multi-spectral images may enable the accurate identification of these two states (managed/unmanaged vegetation over a cropping season), our approach relies on such annual LULC mapping and the subsequent analysis of these maps over multiple years to provide a consistent, field-level accurate mapping of NAAL.

More specifically, we propose to exploit the potential of Sentinel-2 time series for detecting non-active agricultural land, following a supervised approach that relies on several consecutive years of ground truth data registered at field scale, and classical machine learning algorithms. This exploratory study is carried out in South-West Burkina Faso, on a site representative of the sub-humid cereal-based West African farming systems in order to give a thorough insight into the feasibility and potential of the proposed methodology in high-resolution NAAL mapping. We take advantage of an actually available multi-annual *in-situ* reference data base that will be introduced in the next section.

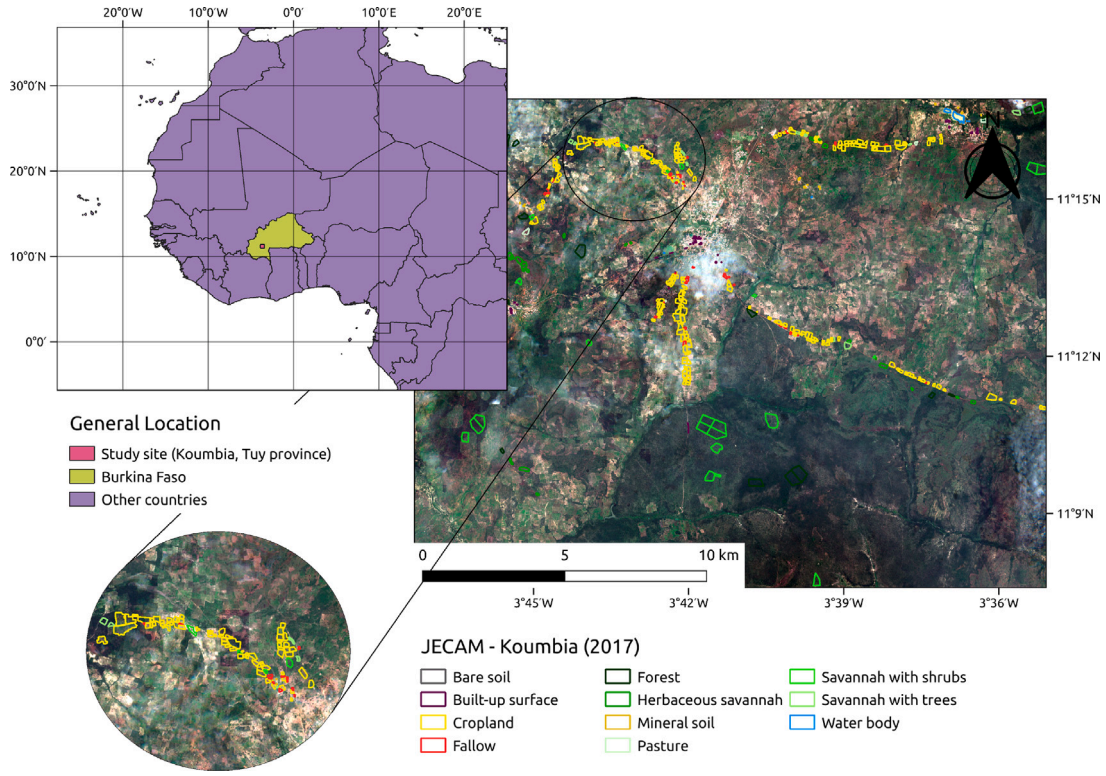

Fig. 1. Location of the Koumbia study site in Burkina Faso (top left), JECAM ground data set polygons (Jolivot et al., 2021) and Sentinel-2 sub-image in 2017 (right), and a zoom-in (bottom left).. (For interpretation of the references to color in this figure legend, the reader is referred to the web version of this article.)

2. Data description

2.1. Study site

Our study site locates in the commune of Koumbia, Tuy Region, in South-Western Burkina Faso (see Fig. 1), covering an area of over 2500 km^2. In this area, rainfall distribution over a year is uni-modal and averaging between 900–1200 mm, which corresponds to typical values in the Sudanese agro-climatic zone (Abdoulaye et al., 2017). Cropping season begins on late April–May and extends till November–December, in concordance with the rainy season. As in most part of the Sahelian area, the study area is characterized by a tree-based cropping system, where multipurpose trees have been deliberately preserved and managed by farmers on agricultural land (Boffa, 1999). The cropping system is rainfed, relying mainly on maize–cotton rotations where cotton is used as cash crop. Other crops include sorghum, millet, oilseed (groundnuts, sesame) and leguminous (e.g. cowpea) crops. Predominant soil textural types are sandy clay loam and sandy loam, accounting for 44% and 54% respectively in the region of study (Miller et al., 2021).

2.2. Reference data set

As reference data, we used the Burkina Faso subset of the recently published JECAM (Joint Experiment for Crop Assessment and Monitoring) harmonized in-situ data set (Jolivot et al., 2021). This ground data set includes land cover and agricultural land use in-situ observations collected annually over the Koumbia site during the 2013–2021 period (on average, c.a. 840 observations per year). More precisely, each object (a polygon) is annotated at both a *land cover* level, using a general nomenclature including the agricultural land in a single class (*cropland*, which includes also "fallow" land), and a set of classes related to natural areas (discriminating *herbaceous savannah* and *natural pastures* from *shrubby* and *woody savannah* and *forests*), *water* bodies and non-vegetated areas (*built-up surfaces* and *mineral soils*). In the JECAM data set, information on the crop type is also available for each polygon within the cropland class. We used this information to build an intermediate-level nomenclature named "Crop group", to keep *fallow* fields and active agricultural land (*cash crop*, *cereals*, *leguminous*, *oilseed*) separated. Details on the final nomenclature along with the surface covered by each class are given in Table 1.

Information for year 2019, originally missing from the published data set, was collected in 2020 by a local agent who carried out a delayed field survey, during which details on fallow land could not be collected.

2.2.1. Satellite and environmental data

On this study we employed L2 A Sentinel-2 (S2) image time series. The Copernicus Sentinel-2 mission includes a constellation of 2 satellites carrying a single multi-spectral instrument (MSI) with 13 spectral channels distributed in the visible/near infrared (VNIR) at 10 m spatial resolution, in short-wave infrared (SWIR) at 20 m spatial resolution, and in complementary bands at spatial 60 m resolution for cloud screening and atmospheric corrections (Drusch et al., 2012). All available images between 2016 and 2021 were downloaded from Theia[1] Land repository, and pre-processed using the open access MORINGA processing chain Gaetano et al. (2019). Image pre-processing includes resampling the SWIR 20 m bands to 10 m resolution, and image time series gap filling of cloudy pixels using multi-temporal linear interpolation as explained in Inglada et al. (2017). Gap-filled images were generated at a 10-day frequency and six vegetation-related radiometric indices (see Table 2) were calculated and appended to the reflectance bands for each timestamp.

[1] THEIA is the French Land Surface Pole gathering academic and public institutions to facilitate the use of Earth observation for monitoring continental surfaces. See https://theia-land.fr for more information.

Table 1
JECAM Koumbia data set area (ha) at *land cover* and *crop group* levels.

Land cover	Crop group	2015	2016	2017	2018	2019	2020	2021
Bare soil		1.60	1.41	0.66	1.33	0.00	3.40	1.90
Built-up surface		6.59	11.48	8.21	8.59	5.98	9.50	9.79
Herbaceous savannah		85.70	102.02	110.90	111.58	62.58	64.45	
Natural pastures		11.25	18.68	12.52	16.88	0.00	43.42	23.26
Shrubby savannah		214.43	229.51	241.94	231.96	214.43	219.04	235.59
Woody Savannah		0.00	21.84	17.10	35.67	0.00	0.00	7.44
Forest		133.70	130.88	142.32	139.77	115.61	155.02	142.67
Water bodies		12.24	12.24	12.24	12.24	12.24	12.24	12.24
Cropland	**Cash**	73.71	105.78	212.01	94.22	102.59	81.16	114.78
	Cereals	171.53	179.51	232.07	159.50	161.14	109.74	172.20
	Leguminous	34.94	39.40	27.33	36.00	17.37	71.90	96.71
	Oilseed	50.04	42.60	35.22	15.63	8.52	28.69	34.08
	Fallow	32.13	20.64	21.79	7.69	0.00	8.74	9.41
Total		865.61	917.49	1077.30	872.65	700.92	809.10	924.28

Table 2
List of the radiometric indices used. Provided bands refer to Sentinel-2 nomenclature ($B2$ is the *blue* band, $B3$ is *green*, $B4$ is *red*, $B5$, $B6$ and $B7$ are *red-edge* bands (700–800 nm), $B8$ is *near infrared* and $B9$, $B10$, $B11$ and $B12$ are *short-wave infrared* bands (950–2200 nm)). The first group corresponds to the multi-temporal indices computed at 10-day frequency over a whole year; The second group refers to the *soil* indices computed for the January–June period.

Annual time-stamp	Index	Formula	Reference
10-day	Normalized Difference Vegetation Index	$NDVI = \frac{B8-B4}{B8+B4}$	Rouse et al. (1974)
	Normalized Difference Water Index	$NDWI = \frac{B3-B8}{B3+B8}$	McFeeters (1996)
	Brightness Index	$BRI = \sqrt{B2^2 + \cdots + B12^2}$	Inglada et al. (2017)
	Modified NDWI	$MNDWI = \frac{B3-B11}{B3+B11}$	Xu (2006)
	Short-wave NDVI	$SWNDVI = \frac{B11-B8}{B11+B8}$	Gao (1996)
	Normalized Difference Red Edge Index	$NDRE = \frac{B8-B5}{B8+B5}$	Barnes et al. (2000)
Seasonal (Jan–Jun)	Redness Index	$RI = \frac{B4^2}{B3^3}$	Mathieu et al. (1998)
	Color Index	$CI = \frac{B4-B3}{B4+B3}$	Mathieu et al. (1998)
	Brilliance Index	$BI = \sqrt{\frac{B3^2+B4^2}{2}}$	Mathieu et al. (1998)
	Brilliance Index II	$BI2 = \sqrt{\frac{B3^2+B4^2+B8^2}{3}}$	Escadafal et al. (1989)
	Normalized Burn Ratio	$NBR = \frac{B8-B11}{B8+B11}$	García and Caselles (1991)

The soil type being a possible driver in the occurrence and duration of fallow practices (Samaké et al., 2005), we also computed for each year the median values of several soil indices using images acquired during the dry season (January–June) when the vegetation has not yet grown and the soil is visible. Four soil indices have been chosen, along with the Normalized Burn Area ratio as a variable describing the occurrence of fires, potentially related to slash-and-burn practices happening during the dry season prior to cultivation. A table resuming the computed indices used in this study, and their formula, is reported in Table 2.

Finally, in order to take into account rainfall in our analysis, we also acquired CHIRPS (Funk et al., 2014) monthly rainfall data reprojected over the S2 grid, at 10 m resolution, using bicubic interpolation (see Fig A.5 in supplementary material.). Besides the fact that a significant downscaling error is likely, rainfall is known to be highly spatially variable in West Africa (Graef and Haigis, 2001; Lebel and Le Barbé, 1997), we make the assumption that these data may relate to the site-scale rainfalls. The assessment of the contribution of each input variable on model decision is part of our analysis.

3. A multi-year land use approach for NAAL mapping

3.1. A multi-year land use approach for NAAL mapping

The main constraint of our approach is the availability of a proper reference data set covering multiple consecutive years, which provides information, for each year and with no ambiguities, on whether a labeled surface belongs to the active cropland, and hence to a *managed* agricultural land class, or to an *unmanaged* class, which can in turn include both non active cropland and natural herbaceous vegetation. Information might also be provided for land cover classes which are more resilient in terms of seasonal variations in vegetation dynamics, information which can be useful to detect and mask out such areas which are less related to the purpose of NAAL mapping. Needing no specific details on these classes, we could complete our annual land cover model by grouping them all under two classes, namely *evergreen* and *non-vegetated*, to address respectively the constant presence and absence of green vegetation.

As already mentioned in the data description section, the JECAM data set provides annual information on both land cover and crop group classes, and it can easily be used to comply to the 4-class model (*managed*, *unmanaged*, *evergreen*, *non-vegetated*) and allow the production of the annual base maps used for multi-annual NAAL identification.

On these premises, the method we intend to propose here is quite straightforward, composed of three stages tackling respectively : (a) the production of annual base maps inferring the 4-class land cover model to the entire area, (b) the application of transition rules for the analysis of land cover trajectories allowing the identification of NAAL, and (c) a suitable processing of the original reference data set to provide a reliable and fair validation of NAAL detection. An overall scheme of the proposed three-stage method is depicted in Fig. 2, a detailed description of each processing block is provided in the following subsections.

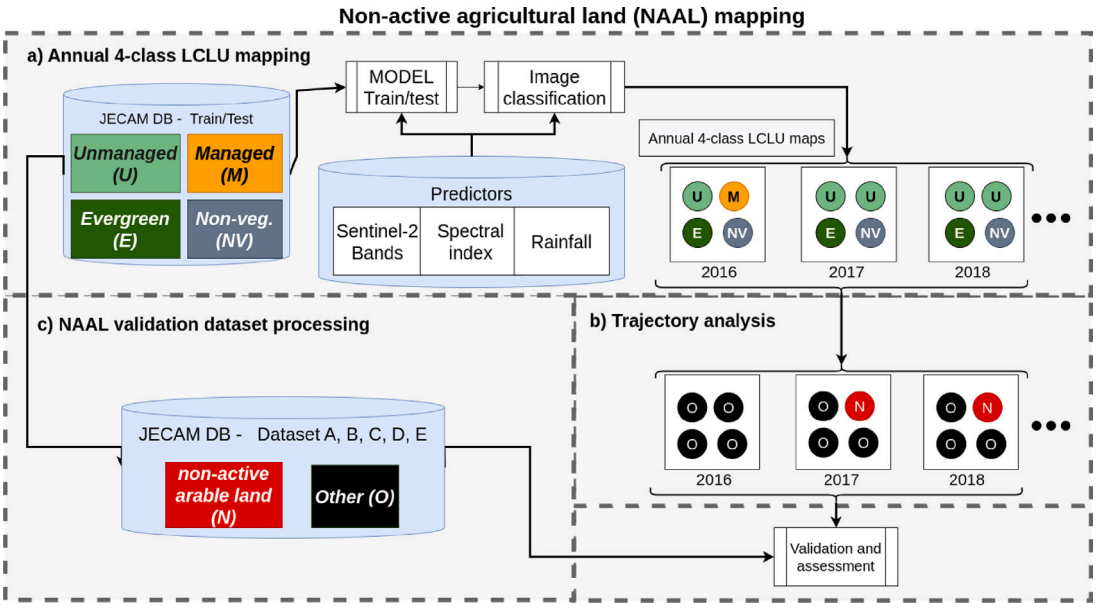

Fig. 2. NAAL mapping general workflow: (a) annual land use mapping and generation of 4-class maps; (b) Trajectory analysis of land use maps and NAAL detection; (c) Reference data set processing for the validation of the NAAL maps.. (For interpretation of the references to color in this figure legend, the reader is referred to the web version of this article.)

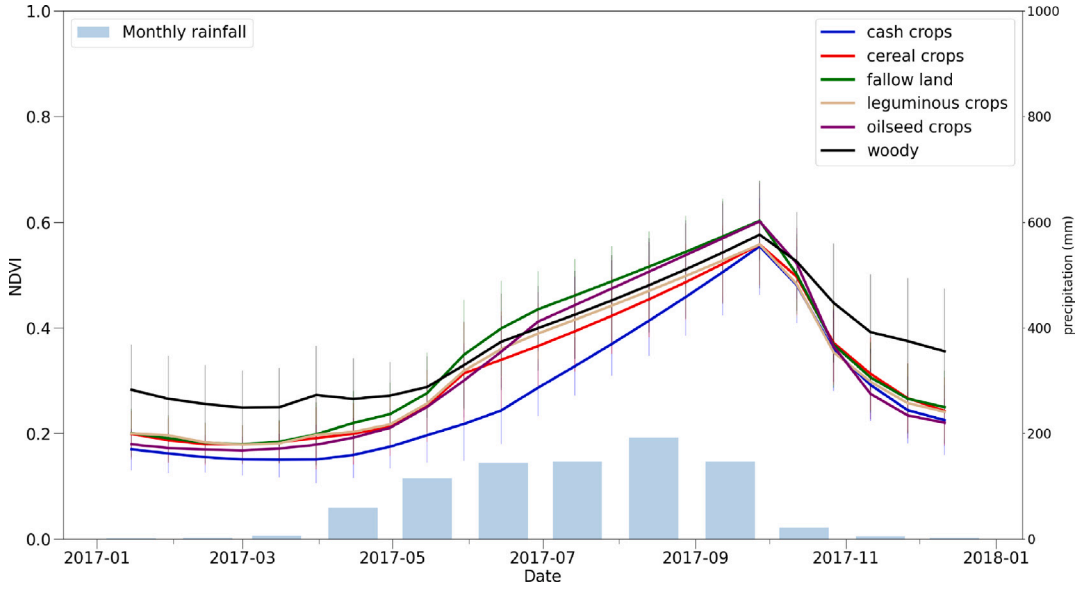

Fig. 3. Average seasonal NDVI profiles calculated with gap-filled Sentinel-2 data and JECAM's Koumbia subset. Rainfall data obtained from CHIRPS monthly data (Funk et al., 2014). Vertical lines represent standard deviation for each LCLU class.. (For interpretation of the references to color in this figure legend, the reader is referred to the web version of this article.)
Source: Adapted from Castro Alvarado (2022).

3.1.1. Sentinel-2 based annual land use mapping

Our first step consists in training a set of annual supervised classification models using the corresponding time series of Sentinel-2 images as a main input. A first straightforward possibility could have been to simply perform a supervised classification directly using the JECAM data set as-is to train the classifier. However, it is clear from Table 1 that a strong class imbalance is present in terms of annotated surface, which may lead to poor performances on less represented classes. This is particularly true for the *fallow* class which, as arguably deductible observing the entangled NDVI profiles shown in Fig. 3 (for year 2017, without loss of generality), is likely to be confused with some active crop class and hence erroneously detected as *managed*, in contradiction to the provided definition of NAAL.

Hence, we here decide to pre-process the JECAM data set prior to the supervised classification process, by relabeling samples of the active crop classes into a single *managed* class (namely the *cash crops, cereals, leguminous and oilseed* classes), and grouping *fallows* with other deciduous vegetation classes (namely *herbaceous, shrubby savannah and pastures*) into the *unmanaged* class. *Woody savannah* and *forest* fall into the *evergreen* class, while the *non-vegetated* class includes all constantly non-vegetated areas (*bare soil, built-up, water bodies*). We report in Fig. 4 the final number of pixels per class after the proposed class grouping and the rasterization of the source vector layer using the

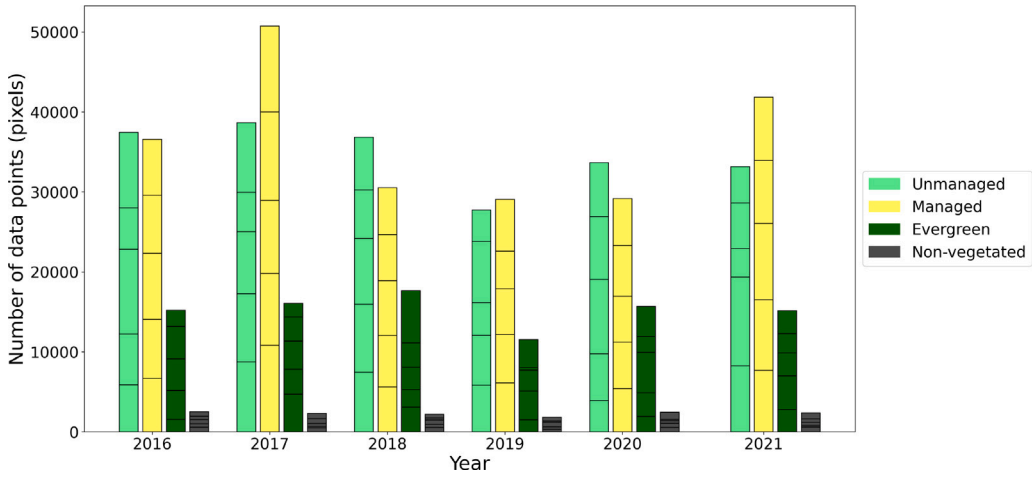

Fig. 4. Number of data points in pixels (after rasterization using the Sentinel-2 10-m grid as spatial reference) for all years and separated by management land use classes. Bar splits represent the proportion of pixels employed in each cross validation fold, see Section 3.2.1.. (For interpretation of the references to color in this figure legend, the reader is referred to the web version of this article.)

Sentinel-2 10 m grid. As expected, the final result shows a much more balanced configuration of class samples, especially between the *managed* and *unmanaged* classes whose transitions through subsequent years are susceptible to trigger the detection of NAAL areas. The overall classification problem is simplified, the least represented classes being the *non-vegetated* and *evergreen* areas which are in turn the easiest to discriminate using radiometric information.

Following an ensemble classification strategy based on the Random Forest algorithm, we decide to use the whole gap-filled time series, along with the derived indices (vegetation-related and soil) as well as rainfall data as predictor variables. A detailed description of the experimental setting of this phase along with an insight on the importance of such variables is provided in the experimental section.

3.1.2. Trajectory analysis for NAAL mapping

Annual 4-class maps provided in previous step over the available time span, say X_t with $t \in \{1, \dots, n\}$, are then employed for the analysis of trajectories implying classes *managed* (M) and *unmanaged* (U) at pixel level to derive the set of $n-1$ NAAL (N) maps Y_t over $t \in \{2, \dots, n\}$ (as a consequence of our causal inter-annual analysis, NAAL identification for the first year of available reference data cannot be computed). Our trajectory hypothesis is quite simple, and based on the following two main rules (see the right-upper part of Fig. 2):

1. any transition from *managed* to *unmanaged* over two subsequent years on a pixel in a location (u, v), say $X_{i-1}(u, v) = M$ and $X_i(u, v) = U$, implies "flagging" a pixel as NAAL on year i, say $Y_i(u, v) = N$;
2. if a pixel is flagged as NAAL for a given year, any subsequent *unmanaged* label on the same pixel is automatically classified as NAAL on the output to maintain temporal and spatial consistency, say:

$$Y_i(u, v) = N, X_j(u, v)|_{j \in i+1, \dots, n} = U \Rightarrow Y_j(u, v) = N$$

In order to reduce possible ambiguities, and on the hypothesis that classes which are less reliant on vegetation dynamics are usually more accurately discriminated, occurrences of either the *evergreen* and *non-vegetated* class on a pixel over time lead to the automatic classification of this pixel as non-NAAL (O) for the whole period. This is done under the implicit hypothesis that no significant changes (such as artificialization or tree plantations) have taken place over the period.

3.1.3. NAAL validation and assessment

In the proposed NAAL classification workflow, a major issue is represented by the necessity to work out a test reference data set to validate the methodology and assess the accuracy of the NAAL maps output by the multi-year trajectory analysis. Matter of facts, we do not dispose of a multi-annual data base of properly annotated NAAL fields. In principle, we could limit our validation to the original JECAM data set and consider the *fallow* class for NAAL assessment. Yet, only relying on this would be unfair, since much more of the arable land could be *de facto* included into the wider NAAL class, including a part of the fallow land which has been annotated as belonging to another deciduous vegetation class because of missing explicit information on cropping practices.

However, it is possible to derive some NAAL-specific validation set from the original JECAM data set by applying the same rules that we use for trajectory analysis on land cover maps, using objects from the data base instead of map pixels, and the intersection of objects over multiple years to track transitions between the *managed* and *unmanaged* classes. This is made possible by the fact that the field survey protocol for the Koumbia site was enforced by taking annotations over the same fields year-by-year to the extent possible. Still, this process is more subtle than it may appear, since a sufficiently large quantity of surface which is overlapping over time and may be labeled as NAAL (which appears to be a small percentage of the area according to the JECAM data set) is needed. Moreover, field boundaries are not static across years, which may lead to a dramatic reduction of usable surface if a simple intersection rule is applied, and in particular a single missing annotation for a given field will make all the data from the relative field unusable.

Thus, we decided to provide several versions of the validation data set, each obtained with a different set of rules for the analysis of the overlaps over time. This goes from a data set obtained by a rigorous intersection of polygons, which is very precise in term of NAAL identification but with a possibly insufficient surface for a reliable assessment, to progressively admitting extrapolation of missing data in space and time, in order to extend the total validation surface, and hence the statistical sufficiency, at the price of some "noise" in the resulting data set.

The different processing approaches over the reference data set, rendered so as to comply to our 4-class model for trajectory analysis, are described below and summarized on Fig. 5. All these processes start with a rasterization of the reference polygons, available in vector format, using the Sentinel-2 grid as geometric reference. As already mentioned, all proposed strategies aim at the relabeling of the whole

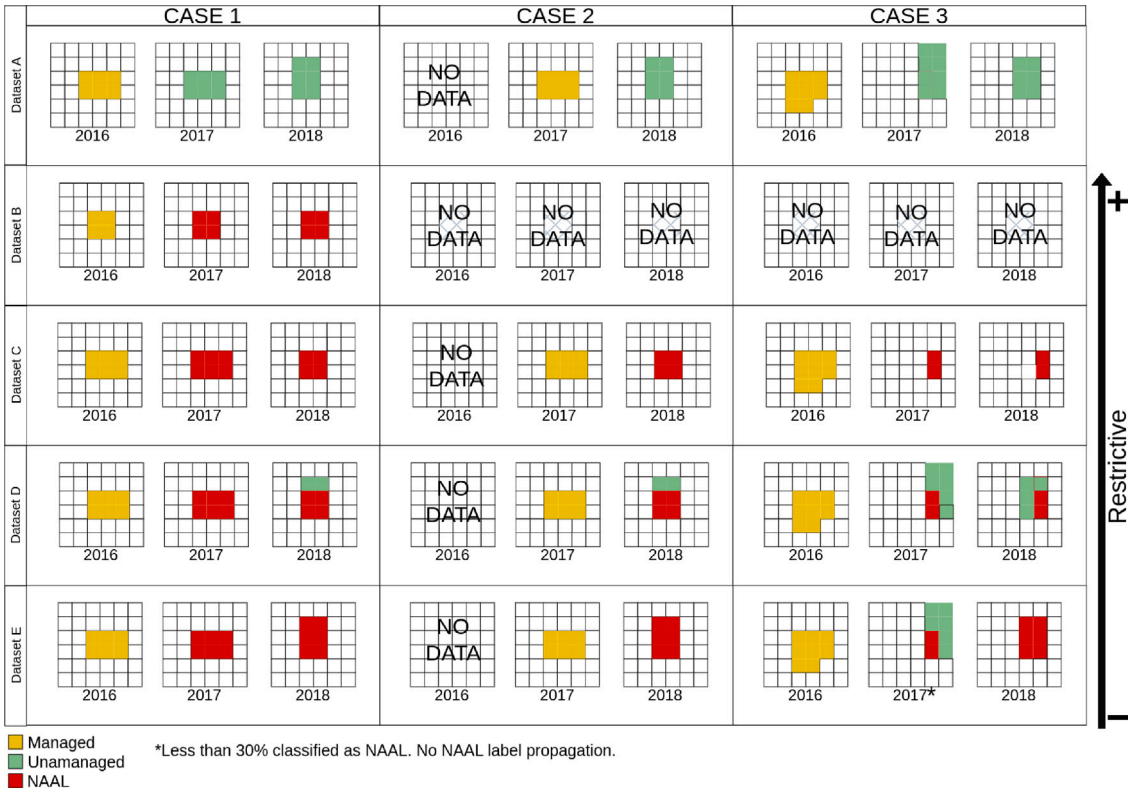

Fig. 5. Illustrative scheme of validation data set processing through 3 examples over 3 consecutive years: Case 1 with no missing years, Case 2 with first year missing, and Case 3 with no stable field boundaries across years considered. Data set A corresponds to the rasterized version of the original JECAM data set, relabeled to fit to the 4-class model (*managed, unmanaged, evergreen, non-vegetated*).. (For interpretation of the references to color in this figure legend, the reader is referred to the web version of this article.)

set of reference pixels from the 4-class nomenclature used for annual mapping to a binary (NAAL vs. non-NAAL) nomenclature based on the same transition rules applied for trajectory analysis. This means that all reference pixels that, for a given year, are not concerned by a relabeling to NAAL are grouped in the unique antagonist *non-NAAL* class. Obviously, the resulting data sets are expected to be strongly unbalanced (NAAL accounts only for a small percentage of the whole area), but in this case the unbiased assessment of the detection of NAAL areas will eventually be possible using per-class figures (*precision*, *recall* and *F1-score*).

Data set A : Original JECAM data set. This validation set is simply made up of the original JECAM Koumbia data set in which the objects are relabeled to fit the 4-class trajectory model. No spatial or temporal modification is applied on the source data. This represents the original data set where only "fallow" fields are considered as NAAL data. There is no data alteration on this case.

Data set B : Strictly reliable surfaces. This is the case when the rigorous multi-annual intersection of reference objects is performed, basically retaining only the most reliable surfaces. In other words, only those pixels where data is available in all consecutive years are considered for trajectory analysis and NAAL relabeling. Any point with missing data for a given year is dropped out of the data set.

Data set C : Locally reliable surfaces. In this scenario, we make the implicit assumption that the validity of a surface for a given year only depends on its past validity. This means that, for a given year, the intersection is only performed with the surface of the overlapping object in the previous year. In this way, all pairs of pixels from two consecutive years that are eligible to be relabeled to NAAL are taken into consideration, regardless of what happened before or after, while the portion of object which is non comparable is discarded. Compared to *data set B*, this data set do not guarantee that a comparable set of surfaces are used for validation year-by-year, leading to possible discrepancies in the multi-annual assessment strategy.

Data set D : Sub-field NAAL relabeling. Here, we basically propose the same logic than for *data set C* at pixel level, with the exception that the portions of objects which are left out from an intersection between two consecutive years are not discarded, and can still be used for NAAL relabeling in subsequent years. Alternatively said, relabeling can occur at sub-field level.

Data set E : field-level NAAL extrapolation. Based on the observation that field boundaries can move through time, and considering how densely cultivated the area is, for this data set we make the underlying hypothesis that, if a certain field is known to have been actively cropped on year Y_i, a newly annotated *unmanaged* field on $Y_i + 1$ whose surface is only partly overlapping with the past year's field is probably a whole NAAL field. Hence, similarly to *data set D*, in this case we still consider pairwise overlaps between consecutive years and no data is lost from the source objects after processing. However, relabeling to NAAL can be propagated to an entire object if the intersection of the given object with the one from the previous year is larger than a given threshold in terms of area percentage, here heuristically fixed to 30%.

A resume of the total number of NAAL pixels for each validation data set and per-year is reported in Fig. 6, along with the percentage it represents with respect to the full data set (including non-NAAL pixels). Note that, by only retaining the strictly reliable surfaces, data set B systematically provide a severe selection of NAAL pixels w.r.t. the total samples, but the other strategies which try to extrapolate NAAL areas at the plot scale progressively tend to first restore the original amount and ratio observable in the data set A (actual *Fallow* fields w.r.t. the total annotated surface), then add some potential NAAL surface in reasonable measure (within a factor of 2). The slight drop in the amount of NAAL pixels in 2020–21 is due to the absence of *Fallow* annotated polygons in the original JECAM data base in 2019.

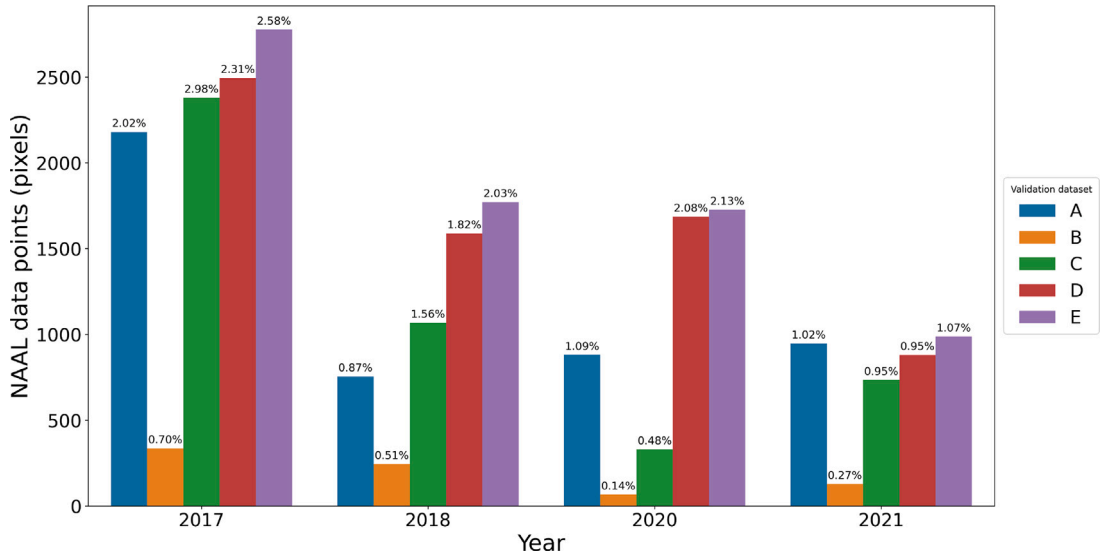

Fig. 6. Total number of NAAL Sentinel-2 pixels in the validation data sets before (A) and after (B to E) processing. The validation data set A corresponds to the JECAM original data set in which the NAAL data pixels correspond to the "Fallow" polygons. For the record, only the cropped fields were registered for year 2019. Values on top of bars show the proportion of NAAL pixels over the total amount of available pixels for that given validation data set and year.. (For interpretation of the references to color in this figure legend, the reader is referred to the web version of this article.)

3.2. Implementation of the approach

3.2.1. Annual LULC maps

For the production of annual 4-class land use maps reliable enough to enable trajectory analysis for NAAL detection, we carried out a strategy based on multiple per-year Random Forest (RF) classifications. Such solution deemed necessary to cope with the relatively low quantity of available annotated surface, especially if compared to the complexity of the landscape and the dimensionality of the input variables (593 variables per pixel in total), as well as to ensure comparability among the different maps.

More precisely, for each available year (2016–2021, no full Sentinel-2 time series was available before 2016), we opted for a 5-fold cross validation approach by dividing the 4-class reference data set derived by the original JECAM Koumbia subset (see Section 3.1) into 5 randomly selected subsets of equal size. To avoid spatial auto-correlation biases in the validation process (Ploton et al., 2020), the sampling of data for the generation of folds happens at the polygon level, following a stratified approach to ensure that the percentage of selected polygons is preserved in each class to the extent possible. We hence make the underlying assumption that, within each class, polygons have comparable areas (same order of magnitude), i.e. the distribution of samples across folds at pixel level will not differ significantly. Bar splits in Fig. 4 show how the polygon-level fold sample selection translates into numbers of reference pixels in per fold/class/year.

As a reminder, cross validation consists in training the same classifier over k different training sets, each one being a unique combination of $k-1$ out of k folds, and validating its performances using the corresponding spare fold. k being equal to 5 in our case, we dispose of 5 RF models per year. Concerning the parametrization of the RF classifiers, for all of them we set the number of trees in forest to 400, and the minimum number of samples required to split an internal node to 25 (with no limit to the depth of the trees). For each year, the resulting RF models have been used to provide 5 different membership probability maps, containing each the probability assigned by one model to any given pixel to belong to any of the 4 land use classes considered, (*managed, unmanaged, evergreen or non-vegetated*). We then generated an annual 4-class map by averaging the probability maps of the 5 models and labeling pixels according to the class with the highest probability. Variable importance (averaged over folds as well) was also computed for each year in order to identify the main predictors and check for consistency across years. Additionally, maximum per-pixel class probability was used as a proxy for identifying zones of lower model certainty.

3.2.2. NAAL mapping

Once 4-class maps were generated we perform the trajectory analysis as described in Section 3.1.2 via custom scripts written on Python 3.8.

4. Experimental results

4.1. Annual LULC maps

The Random Forest trained models were employed for generating 4-class land use maps for the entire study site (see example in Fig. 7 for 2017). The average overall accuracy (OA) across all years considered (2016–2021) was of 91.4%, whereas the average user accuracy (UA) and producer accuracy (PA) across period considered and all classes was 91.7% and 87.3% respectively (full report of map accuracies is provided in Table A.1 in supplementary material). Classwise minimum F1-scores values are 0.91, 0.86, 0.80 and 0.75 for *managed*, *unmanaged*, *evergreen* and *non-vegetated* class respectively, and with *managed* and *unmanaged* classes being consistently the classes with the best scores across all the considered period (Fig. 8).

Per-year variable importance averaged across models is shown in Fig. 9. In order to simplify the reading of such list, the importance for all multi-temporal variables has been averaged over time (e.g. B4 is the average importance of every 10-day Sentinel-2 red bands), but the maximum value of these variables over time is also depicted in red. We here observe that the "hierarchy" of such importance is globally stable over the years, with bands from the red and SWIR spectrum, along with some vegetation indices (NDVI, NDRE) steadily occupying the highest places in the list. Noticeably, both soil indices (RI and CI in particular) and rainfall data have a relatively high importance compared to the large number of spectral variables. Of course, maximum values show that if we consider individual timestamps for each variable, the absolute importance is higher for several spectral bands and indices, but still both external sources of information have a significant and systematic impact in all years' model decisions. For rainfall data in particular, which varied significantly across years considered (see Fig A.5 in supplementary material), band importance results support the hypothesis

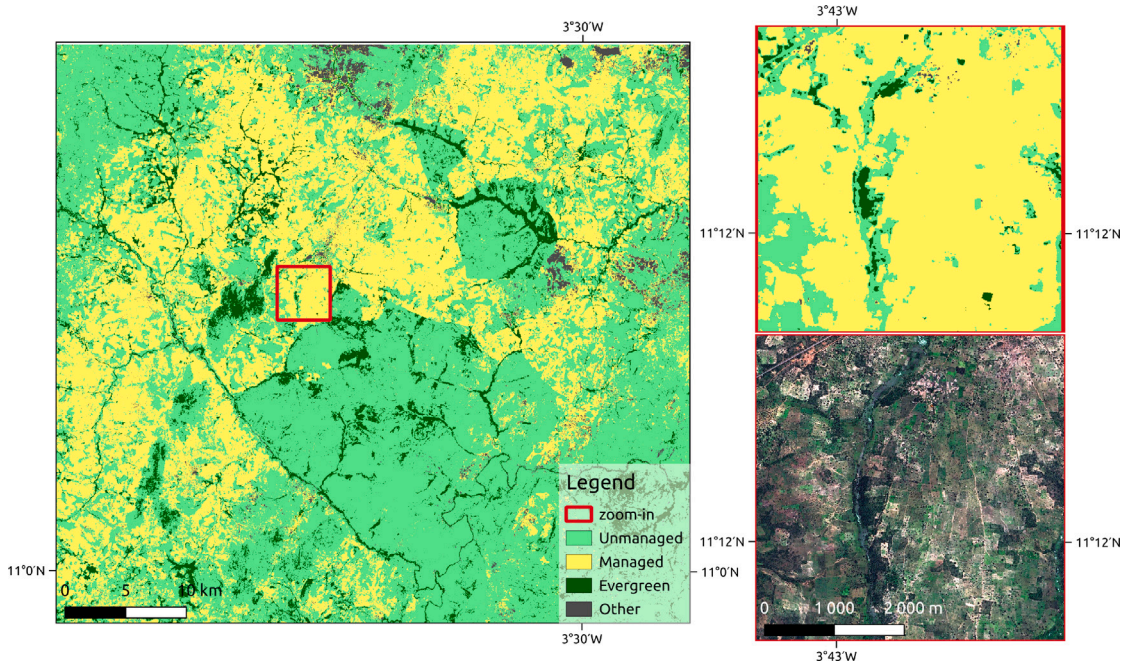

Fig. 7. Annual 4-class resulting land use map for Koumbia site in 2017. On the right, zoom-in and corresponding SPOT 6 ©Airbus DS 2017.. (For interpretation of the references to color in this figure legend, the reader is referred to the web version of this article.)

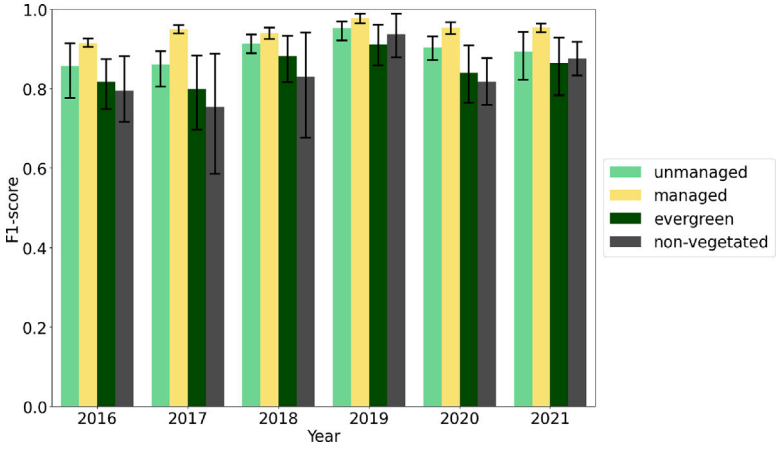

Fig. 8. Average and standard-deviation (error bars) F1-score of annual management land use class, calculated for the five trained Random Forest model's predictions.. (For interpretation of the references to color in this figure legend, the reader is referred to the web version of this article.)

that even at low resolution such information may impact the quality of annual mapping of *managed/unmanaged* surfaces, independently of inter-seasonal variations.

Some interesting elements also come out watching at the maximum class probability map in Fig. 10, which has also been averaged over years. As one might expect, classifier confidence is higher in areas close to the location of reference polygons, even if the average membership probability can also be high in areas where the reference data density is low. However, a pattern of confidence drop is observed across the administrative boundaries of the Koumbia commune. This spatial pattern may be related to shifts in the landscape outside of the commune, in which reference data loses part of its representativeness.

4.2. NAAL mapping and validation

Once the 4-class annual maps have been produced for the 2016–2021 timespan, the trajectory analysis described in Section 3.1.2 was applied to provide NAAL maps over the 2017–2021 period. NAAL map for 2017 is depicted in Fig. 11 where, for sake of clarity, the non-NAAL class (*O* in Fig. 2) has been split in two classes, respectively the *active agricultural land* (AAL) and the *non-agricultural land*, by simply marking as the latter all pixels that have occurrences of either the *evergreen* or *non-vegetated* classes in the annual land use map time series. Observations made for this year remain valid for other years' NAAL maps as well, which are reported in Fig A.1, A.2, A.3, A.4 in supplementary material, with major instabilities only over the low-confidence area of the annual mapping.

At a first glance, it seems evident that the areas corresponding to low classification confidence for annual land use mapping (Fig. 11) present larger portions detected as NAAL, which are more likely to be due to errors in the base maps than to a true switch in agricultural land use in these areas. Things seem more plausible in the area within the Koumbia commune boundaries, also considering prior knowledge on the study site (NAAL accounts in average for c.a. 10% of the total arable land). However, the zoom in the right-upper part of Fig. 11 highlights that, apart from some expected salt-and-pepper artifacts, two different spatial contexts emerge concerning NAAL detection, either (a)

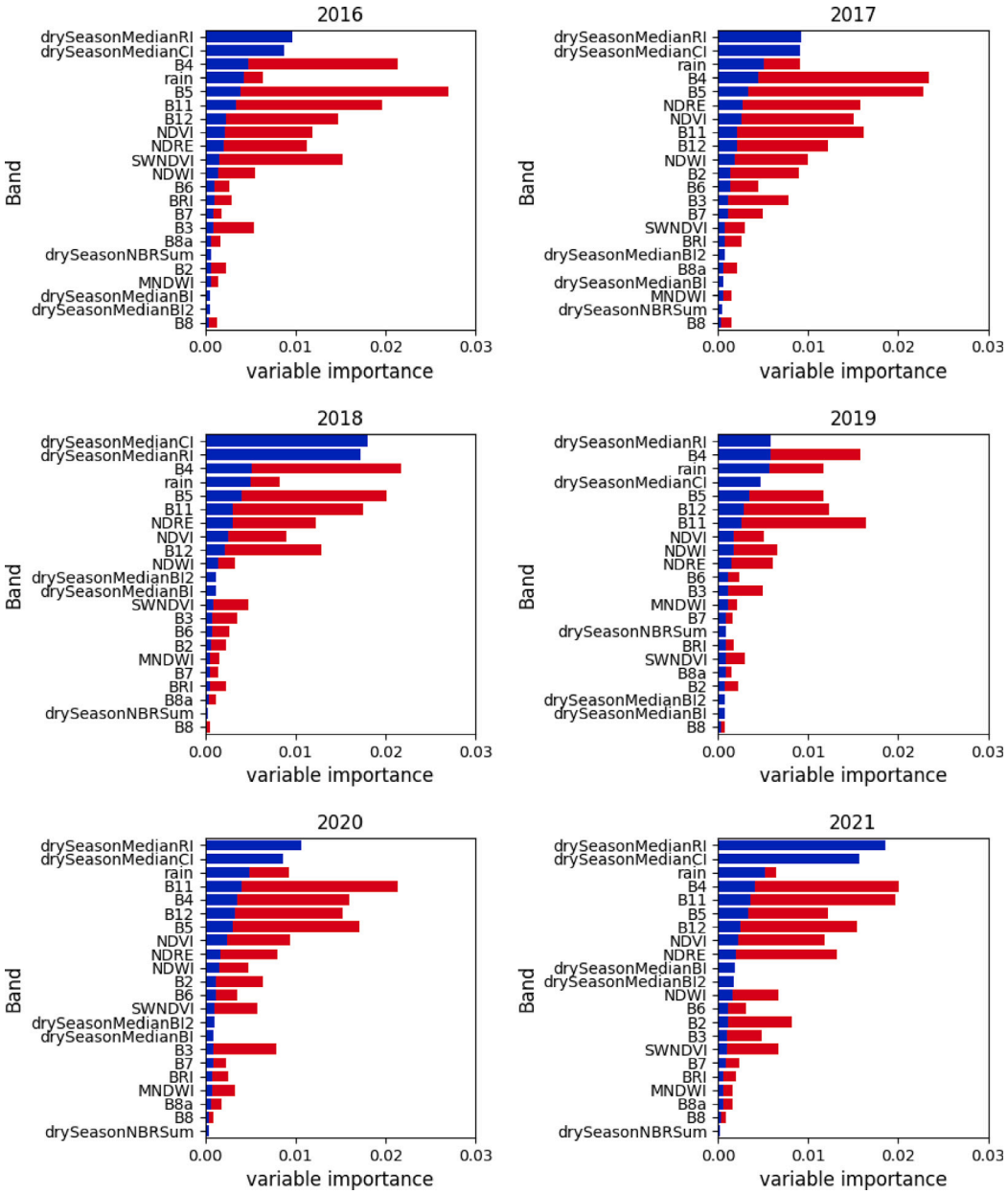

Fig. 9. Per-year average and importance of variables for the Random Forest land use classification models. The importance values of the 10-day variables averaged over the year are represented in blue, and the annual maximum values are reported in red. (For interpretation of the references to color in this figure legend, the reader is referred to the web version of this article.)

in the form of suitably shaped fields within AAL (red regular patches surrounded by yellow), or (b) in transition areas between the AAL and the *non-agricultural* class (red irregular patches along black patches). Some details on field-scale NAAL detection are depicted in Fig. 12, where it is possible to appreciate, in different years and spatial contexts, the correspondence between sets of connected pixels (field-like shaped) detected as NAAL in a given year (right column) and the corresponding field appearance on a very high resolution scene (left column) acquired the same year, at the peak of the growing season. In contrast, artifacts on transition areas may be partly caused by errors in the base mapping due to mixed or misaligned pixels in S2 time series. All this makes reasonable the hypothesis of a significant commission error on these results, and motivates the efforts done in further numerical assessment.

Accuracies (F1-scores) relative to the detection of the NAAL class using the different validation data sets (see Section 3.1.3) are reported in Fig. 13(a) for each year (2019 is skipped since no *fallow* samples are available for data set A), and averaged over the period in Fig. 13(b), along with uncertainties. A full summary of indicators is reported in Table A.1 in supplementary material. Note that due to the large class unbalance in the all reference data sets (NAAL only accounts for 5 to 10% of the annotated surface) we only present per-class accuracy metrics for the NAAL class, since the non-NAAL class achieves always a very high score (close to 1).

First of all, non surprisingly, data set A is the one providing the poorest accuracy figures, with a F1-score over NAAL averaged over the period of analysis around 0.53, with the exception of 2017 when a satisfying score of 0.76 is reached. One may think that this may be due to the missed detection (*omission* error) of older fallows, which would in principle require a "bootstrap" period of five years (according to the agreed-upon definition) to be properly covered by our trajectory model. However, looking at Table 3 it is clear how the low F1-score is mainly due to a systematically low user's accuracy, hence to a high *commission* error. Indeed, in the JECAM database a field is annotated as *fallow* only if a history of active cropping is explicitly known, otherwise non-active

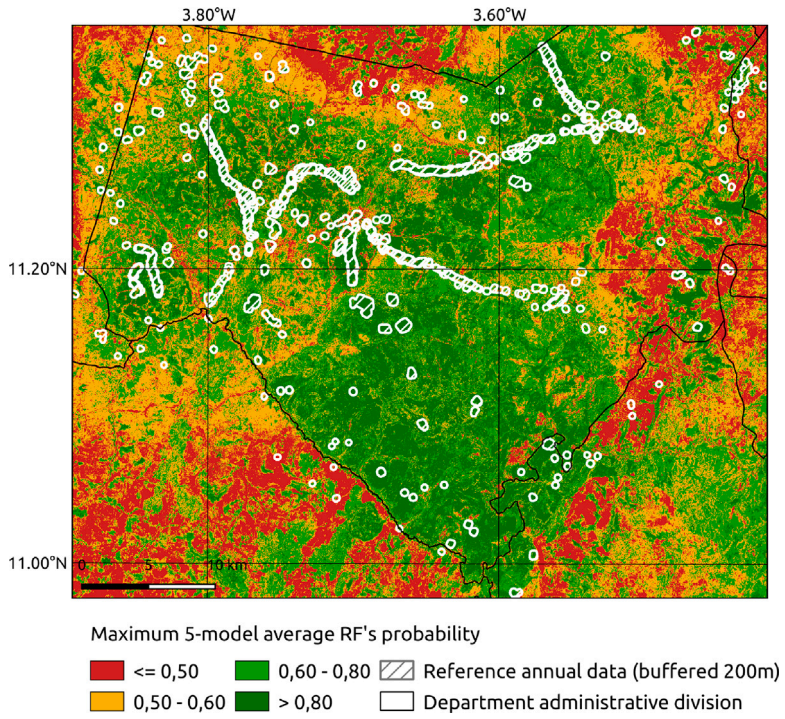

Fig. 10. Average annual maximum Random Forest land use class probability for the 2016–2021 period. Pixel value represents the maximum probability among the four classes considered. The white polygons correspond to all available years of data from JECAM reference data overlapped and with a 200 m buffer. (For interpretation of the references to color in this figure legend, the reader is referred to the web version of this article.)

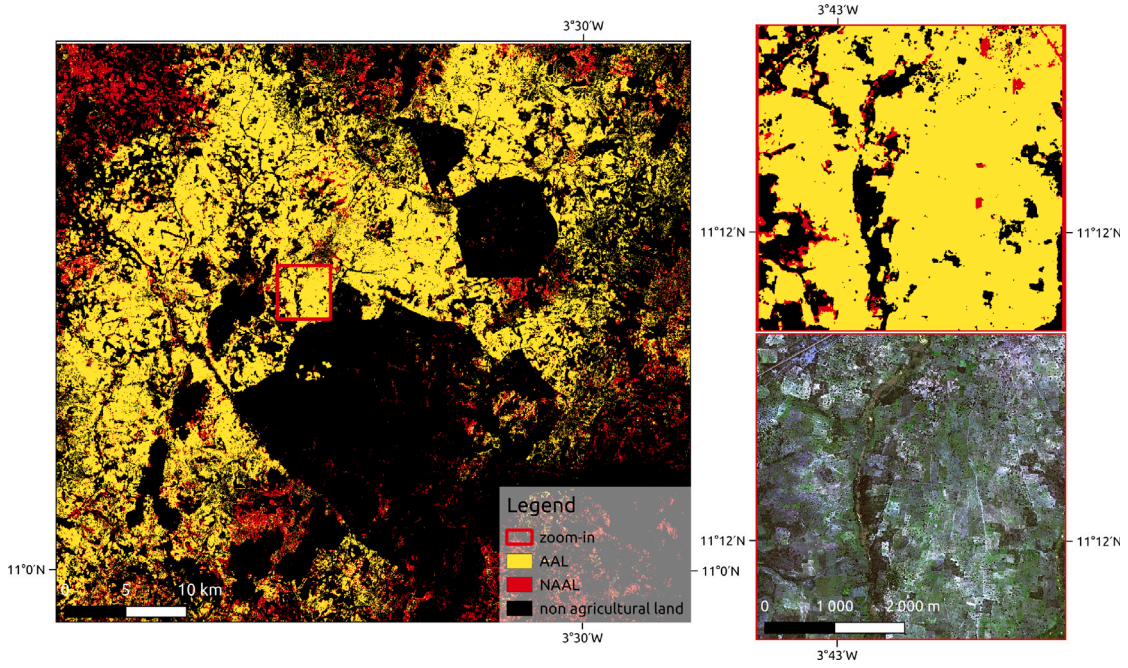

Fig. 11. Annual non-active land (NAAL) map for Koumbia site in 2017. On the right, zoom-in and corresponding SPOT 6 image ©Airbus DS 2017.. (For interpretation of the references to color in this figure legend, the reader is referred to the web version of this article.)

cropland fields fall back into the *herbaceous vegetation* class. This again seems to confirm the hypothesis that not all of the NAAL are correctly represented in the original reference database as *fallow* land, making it necessary to validate NAAL mapping with a different strategy.

Accuracies improve significantly when validating using data set B (strictly reliable surfaces), with an average score of more than 0.8 over the period. However, looking at the number of available reference data points in Fig. 6, we must face the evidence that this value might not be statistically sufficient, as testified by the larger uncertainty. Moreover, this validation potentially suffers from a positive bias due to the fact that, although the two data sets have a different nomenclature (*managed/unmanaged* vs. *NAAL/non-NAAL*) and data distribution among classes, the validation data points belong to the training surface used for annual land use classification. As expected, accuracy values progressively drop when validating over the augmented validation data sets C/D/E, attaining average F1-scores ranging from 0.68 to 0.59, but since they rely on a greater number of validation samples (Fig. 6) the uncertainty is reduced as well.

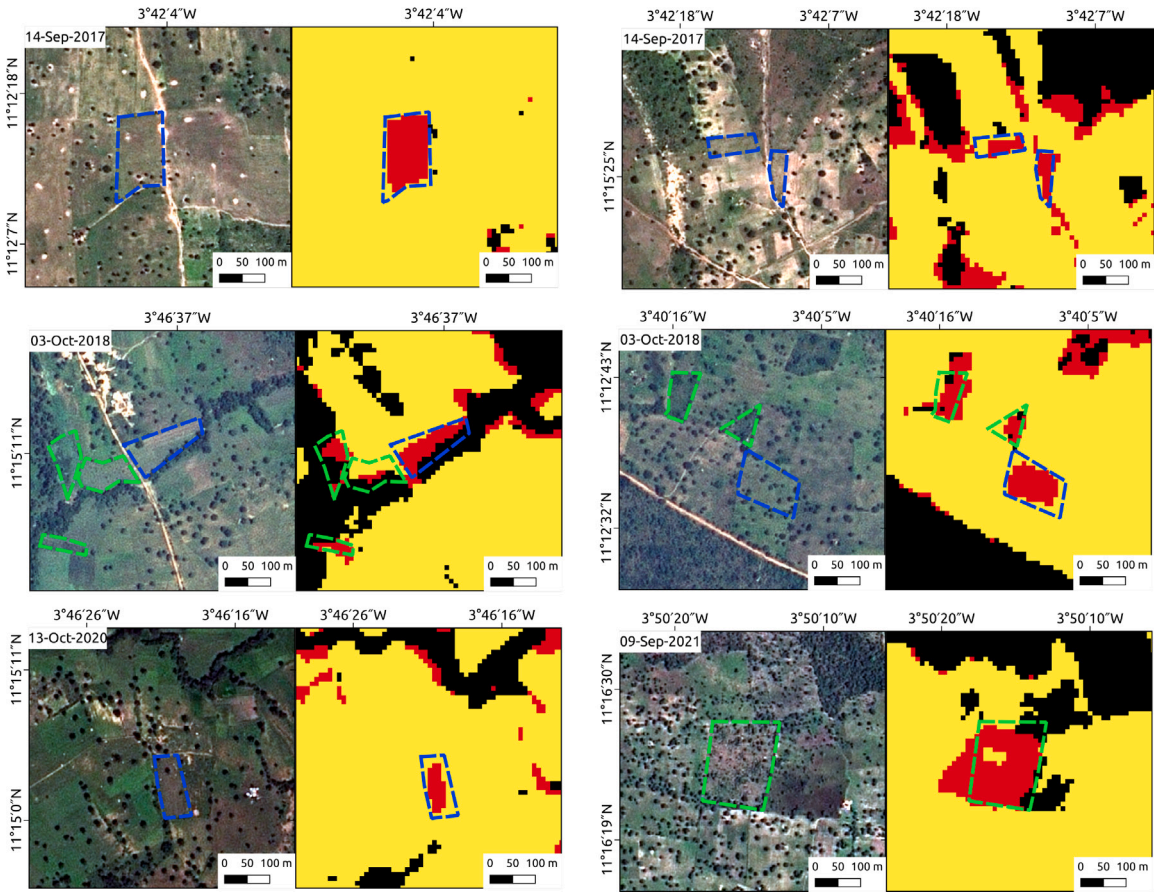

Fig. 12. Multiple samples of NAAL mapping at field scale and different years. For each sample, the image on the left is a very high resolution acquisition (SPOT6/7) which has also been used for field delineation in the JECAM data set (Jolivot et al., 2021); Dotted blue lines have been added to highlight photo-interpreted fields for which NAAL reference data was available for that given year. Dotted green lines represents fields for which no reference data was available that given year. All the fields shown here for which a reference polygon existed was correctly labeled as "NAAL". (For interpretation of the references to color in this figure legend, the reader is referred to the web version of this article.)

Table 3
Annual NAAL maps accuracy metrics (UA, PA and OA stand for user's accuracy, producer's accuracy and overall accuracy respectively) calculated with the five validation data sets.

Validation	Year[a]	UA	PA	OA	F1-score	Kappa
A	2017	0.86	0.67	0.99	0.76	0.75
	2018	0.44	0.81	0.99	0.57	0.57
	2020	0.23	0.72	0.97	0.35	0.34
	2021	0.39	0.71	0.99	0.50	0.49
B	2017	1.00	0.60	1.00	0.75	0.75
	2018	0.99	0.80	1.00	0.89	0.89
	2020	1.00	0.61	1.00	0.76	0.76
	2021	0.99	0.85	1.00	0.92	0.92
C	2017	0.96	0.50	0.98	0.65	0.65
	2018	0.97	0.56	0.99	0.71	0.71
	2020	0.99	0.57	1.00	0.72	0.72
	2021	0.38	0.79	0.99	0.52	0.51
D	2017	0.79	0.51	0.98	0.62	0.61
	2018	0.65	0.55	0.99	0.59	0.58
	2020	0.50	0.79	0.98	0.61	0.60
	2021	0.40	0.79	0.99	0.53	0.52
E	2017	0.86	0.50	0.98	0.63	0.62
	2018	0.68	0.50	0.98	0.58	0.57
	2020	0.50	0.77	0.98	0.61	0.60
	2021	0.44	0.78	0.99	0.56	0.56

[a]Notice that for year 2016 no validation as a result of NAAL detection approach employed (see Section 3.1.2).

4.3. Discussion

The results presented above confirm that the multi-annual strategy proposed in this paper may be a viable way to provide the reliable mapping of NAAL surfaces based on Sentinel-2 image time series in the sub-humid West African agrosystems. This is especially true if compared with previous trials of direct annual mapping of NAAL on the same area, even if in a larger land cover mapping scenario, in which the *fallow* class was mostly missed (average F1-scores lower than 0.2) (Gaetano et al., 2019). An extensive validation has been provided using multiple versions of the reference data set, showing that if we keep the most reliable information available on NAAL reference surfaces the measured accuracy is very high (> 80%) considering the fine scale targeted. However, coping with possible biases in such data set, results also show that, enabling different amounts of reference data augmentation based on suitable hypothesis on spatial correlation at field level, performances still remain significantly higher (F1-score ranging from 0.5 to 0.8) if compared with results achieved using an annual supervised classification approach on the same study area. Although this assessment obviously does not yet allow an operational transfer of the proposed method as a decision support tool, we may legitimately state that trajectory-based model proposed here achieve promising results.

Spatial analysis of NAAL maps also confirms that (i) many areas detected as NAAL are compatible to agricultural fields in shape and size (see Fig. 12) and (ii) the overall occurrence of NAAL surfaces, which amounts in average to around 11% of the total arable land (with peaks of 14% years 2019 and 2021) is coherent with the occurrence of fallow

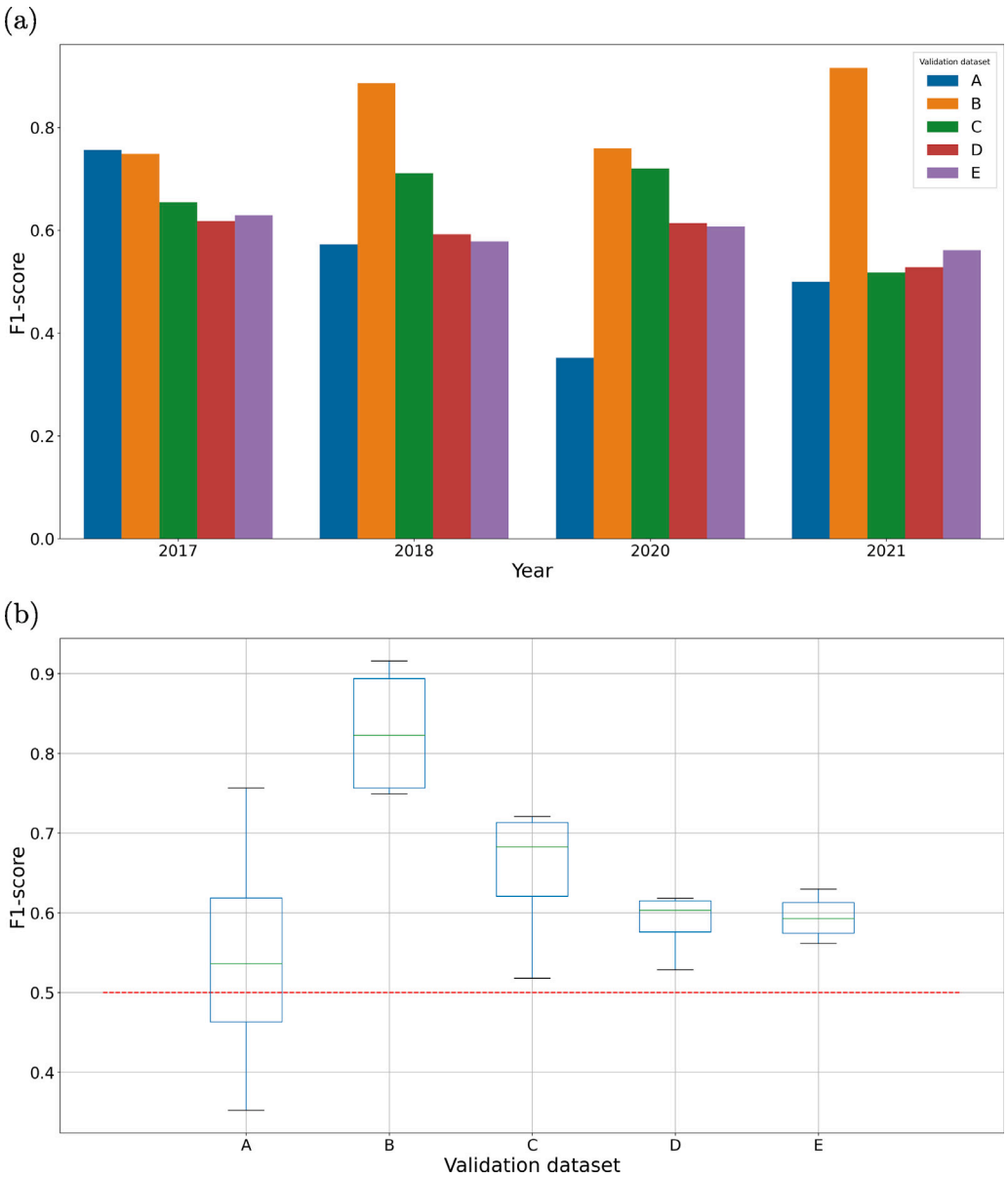

Fig. 13. Sensitivity of the NAAL class accuracy to the validation data set used (A, B, C, D or E) ; (a) The annual average F1-score; (b) Box plot of the mean F1-score calculated over the 2017–2021 period (2019 excluded, see text).. (For interpretation of the references to color in this figure legend, the reader is referred to the web version of this article.)

fields in the JECAM data set across the period. We can hence consider that the proposed methodology is keen to provide locally significant NAAL maps up to the plot scale, contrarily to recent works in fallow mapping (Tong et al., 2020; Dara et al., 2018; Rufin et al., 2022) which, although mainly focusing on large-scale assessment, do not provide evidences of such local significance at the scale of pixel aggregates. Some room for improvement in spatial accuracy could be achieved by post-processing NAAL maps based on prior information on the location and shape of the detected fields. We are currently carrying on some experiments involving field-scale segmentation and object-based NAAL field validation to prove this point.

Despite the mentioned promising outcomes, some limitations have to be pointed out especially concerning the up-scaling potential of this approach. First of all, the availability of a suitable reference database, which must be both precise at field scale and annually updated, is far from standard for the targeted region, and may be costly to produce, also considering that field boundaries are not static in time (Castro Alvarado, 2022). In addition, as shown, even when a proper reference data set is available, ensuring its representativity outside the local scale (e.g. robustly with respect to changes in climate, soil types, vegetation cycles, and all the changes in the captured radiometric information that all this imply) may be hard, making the availability of a broad and extensive data set an absolute necessity.

One may argue that the building of such data base could be addressed through the use of high resolution imagery and photo-interpretation. Yet the feasibility of this strategy relies on the ability of discriminating (i) NAAL from other types natural vegetated spaces and (ii) clear optical differences between NAAL and AAL. These two conditions are rarely met in sub-humid West Africa due to a mainly rainfed-based agriculture and a lack of reliable cropland mapping products (without mentioning the limited availability of exploitable acquisitions during the rainy season). Any improvement in image spatial resolution or temporal frequency within the current range of available products are therefore unlikely to provide substantial improvements in the construction of an extensive enough reference database.

Nonetheless, in this work we provide a first evidence that for a quantification, at least a rough one, of NAAL surfaces the regular (e.g. annual) detection of active cropland vs. other kinds of non-managed deciduous vegetation may suffice, since that would enable the

application of a trajectory model like the one proposed here. Hence, a possibility that we consider worth exploring to address the issue of large-scale NAAL identification is to resort to unsupervised classification techniques for *managed vs. unmanaged* LULC mapping, eventually adapted to specific agro- and eco-systems. One way to proceed could be to exploit the proposed supervised classification workflow to deeply inspect the combination of image-derived variables allowing for the discrimination between these two classes, and design a proper unsupervised methodology to provide such discrimination. In this setting, the deployment of field work for gathering reference data may be based on an agrosystem-scale sampling in representative areas, moving the whole workflow within the range of feasibility.

Further investigation are also being carried out to explore the space of deep-learning based classification methods and assess their performances w.r.t. the legacy Random Forest classifier used here, in particular the methods that explicitly consider the temporal correlation of variables. This could be another way to enhance the robustness of the *managed vs. unmanaged* classification, but could also constitute the base for a direct NAAL discrimination through the analysis of multi-annual satellite images time-series (SITS).

5. Conclusions

Quantification of non-active agricultural land in West Africa is essential to accurately assess agricultural systems on food security and agro-ecological sustainability of current practices.

In this study we proposed a pixel-based methodology that makes use of freely available remote sensing data, multiple years of ground truth data registered *in situ*, and implements a simple 4-class LCLU typology and a multi-annual trajectory model that allows the mapping of Non Active Agricultural Land (NAAL). Our approach showed positive results, improving mapping accuracy of NAAL in the area compared to previous trials and illustrating the importance of the reference data set preprocessing, in time and space, to correctly identify this land use class that is multi-annual in nature. Future works are being put in place to improve annual LULC maps via deep learning techniques and address the issue of the upscaling of the method to larger extents (e.g. the whole sub-humid West Africa).

CRediT authorship contribution statement

Enzo Castro Alvarado: Writing – original draft, Writing – review & editing, Conceptualization, Methodology, Software, Formal analysis, Investigation, Visualization. **Agnès Bégué:** Methodology, Resources, Writing – review & editing, Project administration, Funding acquisition. **Louise Leroux:** Resources, Writing – review & editing. **Raffaele Gaetano:** Writing – original draft, Writing – review & editing, Conceptualization, Methodology, Software, Formal analysis, Investigation, Supervision, Resources, Funding acquisition.

Declaration of competing interest

The authors declare that they have no known competing financial interests or personal relationships that could have appeared to influence the work reported in this paper.

Data availability

Data is freely available and links and reference to it are included in manuscript.

Acknowledgments

Enzo Castro Alvarado received for his work a fellowship from the French National Research Agency under the Investments for the Future Program ANR-16-CONV-0004 (DigitAg), and from CIRAD. The ground data collection was partly funded by CNES (APR TOSCA). The authors wish also to thank the European Space Agency (ESA) for the Sentinel 2 data, Theia pole for the calibration of the Sentinel-2 images, and Bertin Kaboré for collecting the 2019–2021 in-situ data.

Appendix A. Supplementary data

Supplementary material related to this article can be found online at https://doi.org/10.1016/j.jag.2023.103398.

References

Abdoulaye, D., Bruno, B., Bétéo, Z., Hamma, Y., 2017. Impact of climate change on cotton production in Burkina Faso. Afr. J. Agric. Res. 12 (7), 494–501. http://dx.doi.org/10.5897/AJAR2015.10763, URL http://academicjournals.org/journal/AJAR/article-abstract/01E4D7A62764.

Barnes, E.M., Clarke, T.R., Richards, S.E., Colaizzi, P.D., Haberland, J., Kostrzewski, M., Waller, P.M., Choi, C.Y., Riley, E., Thompson, T.L., Lascano, R.J., Li, H., Moran, M.S., Robert, P.C., Rust, R.H., Larson, W.E., 2000. Coincident detection of crop water stress, nitrogen status and canopy density using ground-based multispectral data. In: Proceedings of the 5th International Conference on Precision Agriculture and Other Resource Management. July 16-19, 2000, Bloomington, MN USA.

Bégué, A., Arvor, D., Bellon, B., Betbeder, J., de Abelleyra, D., P. D. Ferraz, R., Lebourgeois, V., Lelong, C., Simões, M., R. Verón, S., 2018. Remote Sensing and Cropping Practices: A Review. Remote Sens. 10 (2), 99. http://dx.doi.org/10.3390/rs10010099, URL http://www.mdpi.com/2072-4292/10/1/99.

Boffa, J.M., 1999. Agroforestry Parklands in Sub-Saharan Africa. (34), Food & Agriculture Org.

Bontemps, S., Defournya, P., Van Bogaert, E., Weber, J.L., Arino, O., 2009. GlobCorine–a joint EEA-ESA project for operational land dynamics monitoring at pan-European scale. In: The 33rd International Symposium on Remote Sensing of Environment. tex.organization: Tucson/Arizona USA.

Brown, C.F., Brumby, S.P., Guzder-Williams, B., Birch, T., Hyde, S.B., Mazzariello, J., Czerwinski, W., Pasquarella, V.J., Haertel, R., Ilyushchenko, S., Schwehr, K., Weisse, M., Stolle, F., Hanson, C., Guinan, O., Moore, R., Tait, A.M., 2022. Dynamic world, near real-time global 10 m land use land cover mapping. Sci. Data 9 (1), 251. http://dx.doi.org/10.1038/s41597-022-01307-4, URL https://www.nature.com/articles/s41597-022-01307-4.

Buchhorn, M., Smets, B., Bertels, L., Roo, B.D., Lesiv, M., Tsendbazar, N.E., Herold, M., Fritz, S., 2020. Copernicus Global Land Service: Land Cover 100m: collection 3: epoch 2019: Globe. http://dx.doi.org/10.5281/zenodo.3939050, URL https://zenodo.org/record/3939050 Type: dataset.

Castro Alvarado, E., 2022. Fallow ID: Characterization and mapping of fallow fields in West-Africa study case using Sentinel-2. Bonn, Germany, URL https://earth.esa.int/living-planet-symposium-2022-presentations/.

Dara, A., Baumann, M., Kuemmerle, T., Pflugmacher, D., Rabe, A., Griffiths, P., Hölzel, N., Kamp, J., Freitag, M., Hostert, P., 2018. Mapping the timing of cropland abandonment and recultivation in Northern Kazakhstan using annual Landsat time series. Remote Sens. Environ. 213, 49–60. http://dx.doi.org/10.1016/j.rse.2018.05.005, URL https://linkinghub.elsevier.com/retrieve/pii/S0034425718302268.

Drusch, M., Del Bello, U., Carlier, S., Colin, O., Fernandez, V., Gascon, F., Hoersch, B., Isola, C., Laberinti, P., Martimort, P., Meygret, A., Spoto, F., Sy, O., Marchese, F., Bargellini, P., 2012. Sentinel-2: ESA's Optical High-Resolution Mission for GMES Operational Services. Remote Sens. Environ. 120, 25–36. http://dx.doi.org/10.1016/j.rse.2011.11.026, URL https://www.sciencedirect.com/science/article/pii/S0034425712000636.

Escadafal, R., Girard, M.-C., Courault, D., 1989. Munsell soil color and soil reflectance in the visible spectral bands of landsat MSS and TM data. Remote Sens. Environ. 27 (1), 37–46. http://dx.doi.org/10.1016/0034-4257(89)90035-7, URL https://www.sciencedirect.com/science/article/pii/0034425789900357.

Estel, S., Kuemmerle, T., Alcántara, C., Levers, C., Prishchepov, A., Hostert, P., 2015. Mapping farmland abandonment and recultivation across Europe using MODIS NDVI time series. Remote Sens. Environ. 163, 312–325. http://dx.doi.org/10.1016/j.rse.2015.03.028, URL https://linkinghub.elsevier.com/retrieve/pii/S003442571500125X.

Estel, S., Kuemmerle, T., Levers, C., Baumann, M., Hostert, P., 2016. Mapping cropland-use intensity across Europe using MODIS NDVI time series. Environ. Res. Lett. 11 (2), 024015. http://dx.doi.org/10.1088/1748-9326/11/2/024015, Publisher: IOP Publishing.

FAO, 2022. Term Portal. FAOTERM. URL https://www.fao.org/faoterm/en/.

Faye, J.B., Hopple, A.M., Bridgham, S.D., 2021. Indigenous farming practices increase millet yields in Senegal, West Africa. Agroecol. Sustain. Food Syst. 45 (2), 159–174, Publisher: Taylor & Francis _eprint: https://doi.org/10.1080/21683565.2020.1815927.

Funk, C.C., Peterson, P.J., Landsfeld, M.F., Pedreros, D.H., Verdin, J.P., Rowland, J.D., Romero, B.E., Husak, G.J., Michaelsen, J.C., Verdin, A.P., et al., 2014. A quasi-global precipitation time series for drought monitoring. US Geol. Surv. Data Ser. 832 (4), 1–12, Publisher: US Geological Survey Reston, VA, USA.

Gaetano, R., Dupuy, S., Lebourgeois, V., Le Maire, G., Tran, A., Jolivot, A., Bégué, A., 2019. The MORINGA processing chain: automatic object-based land cover classification of tropical agrosystems using multi-sensor satellite imagery. In: Living Planet Symposium, LPS 2019. URL https://agritrop.cirad.fr/594650/. Italian Space Agency.

Gao, B.c., 1996. NDWI—A normalized difference water index for remote sensing of vegetation liquid water from space. Remote Sens. Environ. 58 (3), 257–266. http://dx.doi.org/10.1016/S0034-4257(96)00067-3, URL https://www.sciencedirect.com/science/article/pii/S0034425796000673.

García, M.L., Caselles, V., 1991. Mapping burns and natural reforestation using thematic Mapper data. Geocarto Int. 6 (1), 31–37. http://dx.doi.org/10.1080/10106049109354290, Publisher: Taylor & Francis _eprint.

Graef, F., Haigis, J., 2001. Spatial and temporal rainfall variability in the Sahel and its effects on farmers' management strategies. J. Arid Environ. 48 (2), 221–231.

Inglada, J., Arias, M., Tardy, B., Hagolle, O., Valero, S., Morin, D., Dedieu, G., Sepulcre, G., Bontemps, S., Defourny, P., Koetz, B., 2015. Assessment of an Operational System for Crop Type Map Production Using High Temporal and Spatial Resolution Satellite Optical Imagery. Remote Sens. 7 (9), 12356–12379. http://dx.doi.org/10.3390/rs70912356, URL https://www.mdpi.com/2072-4292/7/9/12356. Number: 9 Publisher: Multidisciplinary Digital Publishing Institute.

Inglada, J., Vincent, A., Arias, M., Tardy, B., Morin, D., Rodes, I., 2017. Operational High Resolution Land Cover Map Production at the Country Scale Using Satellite Image Time Series. Remote Sens. 9 (1), 95. http://dx.doi.org/10.3390/rs9010095, URL https://www.mdpi.com/2072-4292/9/1/95 Number: 1 Publisher: Multidisciplinary Digital Publishing Institute.

Jolivot, A., Lebourgeois, V., Ameline, M., Andriamanga, V., Bellón, B., Castets, M., Crespin-Boucaud, A., Defourny, P., Diaz, S., Dieye, M., Dupuy, S., Ferraz, R., Gaetano, R., Gely, M., Jahel, C., Kabore, B., Lelong, C., Le Maire, G., Leroux, L., Lo Seen, D., Muthoni, M., Ndao, B., Newby, T., De Oliveira Santos, C.L.M., Rasoamalala, E., Simoes, M., Thiaw, I., Timmermans, A., Tran, A., Bégué, A., 2021. Harmonized in situ JECAM datasets for agricultural land use mapping and monitoring in tropical countries. Earth Syst. Sci. Data Discuss. 2021, 1–22. http://dx.doi.org/10.5194/essd-2021-125, URL https://essd.copernicus.org/preprints/essd-2021-125/.

Lebel, T., Le Barbé, L., 1997. Rainfall monitoring during HAPEX-sahel. J. Gen. Rainfall Cond. Climatol. L Hydro. 88–189.

Leroux, L., Jolivot, A., Bégué, A., Seen, D.L., Zoungrana, B., 2014. How Reliable is the MODIS Land Cover Product for Crop Mapping Sub-Saharan Agricultural Landscapes? Remote Sens. 6 (9), 8541–8564. http://dx.doi.org/10.3390/rs6098541, URL https://www.mdpi.com/2072-4292/6/9/8541 Number: 9 Publisher: Multidisciplinary Digital Publishing Institute.

Manlay, R.J., Cadet, P., Thioulouse, J., Chotte, J.L., 2000. Relationships between abiotic and biotic soil properties during fallow periods in the sudanian zone of Senegal. Appl. Soil Ecol. 14 (2), 89–101. http://dx.doi.org/10.1016/S0929-1393(00)00052-4, URL https://linkinghub.elsevier.com/retrieve/pii/S0929139300000524.

Mathieu, R., Pouget, M., Cervelle, B., Escadafal, R., 1998. Relationships between Satellite-Based Radiometric Indices Simulated Using Laboratory Reflectance Data and Typic Soil Color of an Arid Environment. Remote Sens. Environ. 66 (1), 17–28. http://dx.doi.org/10.1016/S0034-4257(98)00030-3, URL https://www.sciencedirect.com/science/article/pii/S0034425798000303.

McFeeters, S.K., 1996. The use of the Normalized Difference Water Index (NDWI) in the delineation of open water features. Int. J. Remote Sens. 17 (7), 1425–1432, Publisher: Taylor & Francis _eprint: https://doi.org/10.1080/01431169608948714.

Miller, M.A.E., Shepherd, K.D., Kisitu, B., Collinson, J., 2021. iSDAsoil: The first continent-scale soil property map at 30 m resolution provides a soil information revolution for Africa. PLOS Biol. 19 (11), e3001441. http://dx.doi.org/10.1371/journal.pbio.3001441, URL https://dx.plos.org/10.1371/journal.pbio.3001441.

Ploton, P., Mortier, F., Réjou-Méchain, M., Barbier, N., Picard, N., Rossi, V., Dormann, C., Cornu, G., Viennois, G., Bayol, N., Lyapustin, A., Gourlet-Fleury, S., Pélissier, R., 2020. Spatial validation reveals poor predictive performance of large-scale ecological mapping models. Nature Commun. 11 (1), http://dx.doi.org/10.1038/s41467-020-18321-y.

Qiu, B., Lin, D., Chen, C., Yang, P., Tang, Z., Jin, Z., Ye, Z., Zhu, X., Duan, M., Huang, H., Zhao, Z., Xu, W., Chen, Z., 2022. From cropland to cropped field: A robust algorithm for national-scale mapping by fusing time series of Sentinel-1 and Sentinel-2. Int. J. Appl. Earth Obs. Geoinf. 113, 103006. http://dx.doi.org/10.1016/j.jag.2022.103006, URL https://www.sciencedirect.com/science/article/pii/S1569843222001947.

Rouse, J.W., Haas, R.H., Deering, D.W., Schell, J.A., Harlan, J.C., 1974. Monitoring the Vernal Advancement and Retrogradation (Green Wave Effect) of Natural Vegetation. Technical Report E75-10354, Texas A&M University, URL https://ntrs.nasa.gov/citations/19750020419 NTRS Author Affiliations: Texas A&M Univ..

Rufin, P., Bey, A., Picoli, M., Meyfroidt, P., 2022. Large-area mapping of active cropland and short-term fallows in smallholder landscapes using PlanetScope data. Int. J. Appl. Earth Obs. Geoinf. 112, 102937. http://dx.doi.org/10.1016/j.jag.2022.102937, URL https://linkinghub.elsevier.com/retrieve/pii/S1569843222001340.

Ruthenberg, H., 1974. Farming Systems in the Tropics. Clarendon Press - Oxford.

Samaké, O., Smaling, E., Kropff, M., Stomph, T., Kodio, A., 2005. Effects of cultivation practices on spatial variation of soil fertility and millet yields in the Sahel of Mali. Agricult. Ecosys. Environ. 109 (3–4), 335–345. http://dx.doi.org/10.1016/j.agee.2005.02.024, URL https://linkinghub.elsevier.com/retrieve/pii/S0167880905001246.

Samasse, K., Hanan, N., Tappan, G., Diallo, Y., 2018. Assessing Cropland Area in West Africa for Agricultural Yield Analysis. Remote Sens. 10 (11), 1785. http://dx.doi.org/10.3390/rs10111785, URL http://www.mdpi.com/2072-4292/10/11/1785.

Snapp, S., Rahmanian, M., Batello, C., Calles, T., 2018. Pulse crops for sustainable farms in sub-saharan africa. FAO, http://dx.doi.org/10.18356/6795bfaf-en.

Tittonell, P., Giller, K.E., 2013. When yield gaps are poverty traps: The paradigm of ecological intensification in African smallholder agriculture. Crop Yield Gap Analysis – Rationale, Methods and Applications, Field Crops Res. Crop Yield Gap Analysis – Rationale, Methods and Applications, 143, 76–90. http://dx.doi.org/10.1016/j.fcr.2012.10.007.URL https://www.sciencedirect.com/science/article/pii/S0378429012003346,

Tong, X., Brandt, M., Hiernaux, P., Herrmann, S., Rasmussen, L.V., Rasmussen, K., Tian, F., Tagesson, T., Zhang, W., Fensholt, R., 2020. The forgotten land use class: Mapping of fallow fields across the Sahel using Sentinel-2. Remote Sens. Environ. 239, 111598. http://dx.doi.org/10.1016/j.rse.2019.111598, URL https://linkinghub.elsevier.com/retrieve/pii/S0034425719306182.

Tong, X., Brandt, M., Vang Rasmussen, L., Hiernaux, P., Bech Bruun, T., Reiner, F., M. Abdi, A., M. Herrmann, S., Li, S., Fensholt, R., 2022. Nano-satellites uphold Boserup's theory of smallholder agricultural intensification. http://dx.doi.org/10.21203/rs.3.rs-2041995/v1, URL https://www.researchsquare.com.

Vollset, S.E., Goren, E., Yuan, C.W., Cao, J., Smith, A.E., Hsiao, T., Bisignano, C., Azhar, G.S., Castro, E., Chalek, J., Dolgert, A.J., Frank, T., Fukutaki, K., Hay, S.I., Lozano, R., Mokdad, A.H., Nandakumar, V., Pierce, M., Pletcher, M., Robalik, T., Steuben, K.M., Wunrow, H.Y., Zlavog, B.S., Murray, C.J.L., 2020. Fertility, mortality, migration, and population scenarios for 195 countries and territories from 2017 to 2100: a forecasting analysis for the Global Burden of Disease Study. Lancet 396 (10258), 1285–1306. http://dx.doi.org/10.1016/S0140-6736(20)30677-2, URL https://www.sciencedirect.com/science/article/pii/S0140673620306772.

Wallace, C.S., Thenkabail, P., Rodriguez, J.R., Brown, M.K., 2017. Fallow-land Algorithm based on Neighborhood and Temporal Anomalies (FANTA) to map planted *versus* fallowed croplands using MODIS data to assist in drought studies leading to water and food security assessments. GISci. Remote Sens. 54 (2), 258–282. http://dx.doi.org/10.1080/15481603.2017.1290913, URL https://www.tandfonline.com/doi/full/10.1080/15481603.2017.1290913.

Wu, Z., Thenkabail, P.S., Mueller, R., Zakzeski, A., Melton, F., Johnson, L., Rosevelt, C., Dwyer, J., Jones, J., Verdin, J.P., 2014. Seasonal cultivated and fallow cropland mapping using MODIS-based automated cropland classification algorithm. J. Appl. Remote Sens. 8 (1), 083685. http://dx.doi.org/10.1117/1.JRS.8.083685, URL https://www.spiedigitallibrary.org/journals/journal-of-applied-remote-sensing/volume-8/issue-1/083685/Seasonal-cultivated-and-fallow-cropland-mapping-using-MODIS-based-automated/10.1117/1.JRS.8.083685.full Publisher: SPIE.

Xu, H., 2006. Modification of normalised difference water index (NDWI) to enhance open water features in remotely sensed imagery. Int. J. Remote Sens. 27 (14), 3025–3033. http://dx.doi.org/10.1080/01431160600589179, Publisher: Taylor & Francis _eprint: https://doi.org/10.1080/01431160600589179.

Xu, Y., Yu, L., Feng, D., Peng, D., Li, C., Huang, X., Lu, H., Gong, P., 2019. Comparisons of three recent moderate resolution African land cover datasets: CGLS-LC100, ESA-S2-LC20, and FROM-GLC-Africa30. Int. J. Remote Sens. 40 (16), 6185–6202. http://dx.doi.org/10.1080/01431161.2019.1587207, URL https://www.tandfonline.com/doi/full/10.1080/01431161.2019.1587207.

Yin, H., Prishchepov, A.V., Kuemmerle, T., Bleyhl, B., Buchner, J., Radeloff, V.C., 2018. Mapping agricultural land abandonment from spatial and temporal segmentation of Landsat time series. Remote Sens. Environ. 210, 12–24. http://dx.doi.org/10.1016/j.rse.2018.02.050, URL https://linkinghub.elsevier.com/retrieve/pii/S0034425718300622.

Zhang, M., Wu, B., Meng, J., Dong, T., You, X., 2014. Fallow land mapping for better crop monitoring in Huang-Huai-Hai Plain using HJ-1 CCD data. IOP Conf. Ser. Earth Environ. Sci. 17, 012048. http://dx.doi.org/10.1088/1755-1315/17/1/012048, URL https://iopscience.iop.org/article/10.1088/1755-1315/17/1/012048.

Zhao, Z., Wang, J., Wang, L., Rao, X., Ran, W., Xu, C., 2023. Monitoring and analysis of abandoned cropland in the Karst Plateau of Eastern Yunnan, China based on Landsat time series images. Ecol. Indic. 146, 109828. http://dx.doi.org/10.1016/j.ecolind.2022.109828, URL https://www.sciencedirect.com/science/article/pii/S1470160X22013012.

Zoungrana, I., 1993. Les jachéres nord-soudaniennes du Burkina Faso: 1. Analyse de la reconstitution de la végétation herbacée. In: La Jachére en Afrique de l'Ouest, Montpellier (France), 1991.